Progress In Electromagnetics Research C, Vol. 74, 111–121, 2017

Optimization and Characterization of Negative Uniaxial Metamaterials

Jose A. Avila, Cesar L. Valle, Edgar Bustamante, and Raymond C. Rumpf*

Abstract—Digital manufacturing, or 3D printing, is a rapidly emerging technology which enables novel designs that incorporate complex geometries and even multiple materials. In electromagnetics and circuits, 3D printing allows the dielectrics to take on new and profound functionality. This paper introduces negative uniaxial metamaterials (NUMs) which are birefringent structures that can be used to manipulate electromagnetic fields at a very small scale. The NUMs presented here are composed of alternating layers of two different dielectric materials. The physics of the NUMs are explained and simple analytical equations for the effective dielectric tensor are derived. Using these equations, the NUMs are optimized for strength of anisotropy and for space stretching derived from transformation optics. The analytical equations are validated through rigorous simulations and by laboratory measurements. Three NUMs where manufactured using 3D printing where each exhibited anisotropy in a different orientation for measurement purposes. All of the data from the analytical equations, simulations, and experiments are in excellent agreement confirming that the physics of the NUMs is well understood and that NUMs can be designed quickly and easily using just the analytical equations.

1. INTRODUCTION

3D printing, or direct digital manufacturing, is a rapidly emerging technology in manufacturing [1]. It offers the capability to manufacture parts with extremely complex geometries and parts made of multiple material types, such as dielectrics and conductors [2]. This manufacturing technology opens the door to many possibilities for electromagnetics and circuits [3–8], such as sculpting electromagnetic fields using spatially variant anisotropic metamaterials [9]. In [10], a positive uniaxial metamaterial was designed, manufactured using 3D printing, and characterized in the lab. The structure was composed of a hexagonal array of high-permittivity rods in a low-permittivity background which made the extraordinary axis oriented parallel to the rods. The present work extends this to negative uniaxial metamaterials (NUMs) that are composed of alternating layers of dielectric. These have the extraordinary axis aligned perpendicular to the planes and the ordinary axes aligned parallel to the planes.

Section 2 begins by quickly reviewing the formulation of the effective medium equations [11–13] for calculating the effective tensor elements. For NUMs composed of sufficiently subwavelength layers of dielectric, the equations are exact. Given these equations, the NUM is optimized in two different ways. First, the NUM is optimized for the greatest anisotropy, where the degree of anisotropy is defined as the difference between the extraordinary ε_{e} and ordinary ε_{o} permittivity. Second, the NUM is derived from transformation optics (TO) [14, 15] and optimized for its ability to stretch space. In Section 3, the analytical equations are validated through rigorous simulations that retrieve the effective tensor elements by solving an eigen-value problem [16]. An experimental setup is then designed and simulated to show that the setup can be used to measure the three effective tensor elements. In Section 4, three

Received 9 March 2017, Accepted 10 May 2017, Scheduled 23 May 2017
* Corresponding author: Raymond C. Rumpf (rcrumpf@utep.edu).
The authors are with EM Lab, University of Texas at El Paso, El Paso, Texas 79968, USA.

different NUMs are manufactured by 3D printing, each containing the extraordinary axis in a different orientation. Each sample was measured in the lab to determine the three effective tensor elements. The analytical, simulated, and experimental data are all in excellent agreement showing the physics of NUMs is well understood and that the analytical equations can be used reliably to design NUMs without the need of electromagnetic simulations.

2. ANALYTICAL OPTIMIZATION

2.1. Derivation of Effective Medium Parameters

Analytical expressions for the tensor elements can be derived analytically using effective medium theory [11, 12, 17, 18]. The geometry and definitions for this analysis are summarized in Figure 1. The structure is composed of alternating layers of dielectric that repeat with period Λ. The fill factor f quantifies what fraction of the NUM is composed of material 1 with permittivity ε_1. The effective permittivity tensor elements of the NUM, ε_o and ε_e, are calculated by solving the constitutive relation for permittivity, however the electric field quantities must be averaged over the volume of the NUM.

$$\varepsilon_{\text{eff}} = \vec{D}_{\text{avg}}/\vec{E}_{\text{avg}} \tag{1}$$

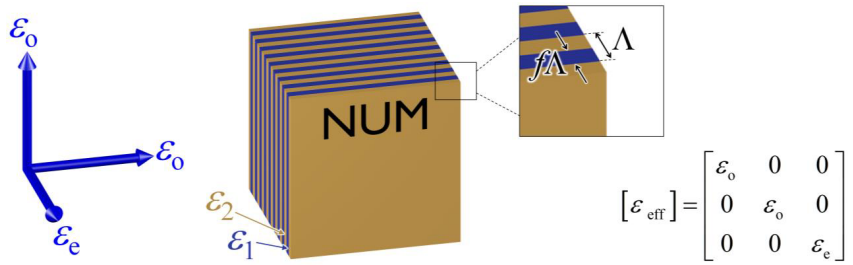

Figure 1. NUM geometry.

The perpendicular polarization is defined to have the electric field aligned parallel to the planes of the NUM. Boundary conditions dictate that the tangential component of the electric field intensity $\vec{E}_{\text{avg}}$ is continuous across the interfaces. This forces the electric field intensity to be virtually constant throughout the NUM as long as the NUM is sufficiently subwavelength. In contrast, the electric flux density $\vec{D}_{\text{avg}}$ is not constant throughout the device because it obeys different boundary conditions. For the perpendicular polarization, the electric flux density takes on different values inside each dielectric. When the NUM is composed of two different materials with permittivity values ε_1 and ε_2, the values of the electric flux density in each dielectric are $\vec{D}_1 = \varepsilon_1\vec{E}_{\text{avg}}$ and $\vec{D}_2 = \varepsilon_2\vec{E}_{\text{avg}}$. Given the volumetric fill factor f of the material described by ε_1, the average electric flux density throughout the NUM can be estimated according to

$$\vec{D}_{\text{avg}} = f\vec{D}_1 + (1-f)\,\vec{D}_2 = f\varepsilon_1\vec{E}_{\text{avg}} + (1-f)\,\varepsilon_2\vec{E}_{\text{avg}}. \tag{2}$$

Substituting this expression for $\vec{D}_{\text{avg}}$ into Eq. (1) gives an expression to estimate the effective permittivity for the perpendicular polarization. This is the ordinary permittivity ε_o of the NUM because the electric field is parallel to the planes of the NUM.

$$\varepsilon_o = f\varepsilon_1 + (1-f)\,\varepsilon_2 \tag{3}$$

The parallel polarization has the electric field intensity $\vec{E}_{\text{avg}}$ aligned perpendicular to the grating grooves. In this second case it is the electric flux density $\vec{D}_{\text{avg}}$ that is continuous across the interfaces. This forces the electric flux density to be virtually constant throughout the NUM as long as the NUM is sufficiently subwavelength. It is now the electric field intensity $\vec{E}_{\text{avg}}$ that is not constant throughout the device and takes on different values inside each dielectric. The values in each dielectric are $\vec{E}_1 = \varepsilon_1^{-1}\vec{D}_{\text{avg}}$

and $\vec{E}_2 = \varepsilon_2^{-1}\vec{D}_{\text{avg}}$. Given the volume fill factor f of the dielectric described by ε_1, the average electric field intensity can be estimated according to

$$\vec{E}_{\text{avg}} = f\vec{E}_1 + (1-f)\,\vec{E}_2 = f\varepsilon_1^{-1}\vec{D}_{\text{avg}} + (1-f)\,\varepsilon_2^{-1}\vec{D}_{\text{avg}}. \tag{4}$$

Substituting this expression for $\vec{E}_{\text{avg}}$ into Eq. (1) gives an expression to estimate the effective permittivity for the parallel polarization. This is the extraordinary permittivity ε_{e} of the NUM because the electric field is perpendicular to the planes of the NUM.

$$\varepsilon_{\text{e}}^{-1} = f\varepsilon_1^{-1} + (1-f)\,\varepsilon_2^{-1} \tag{5}$$

Putting these together, we arrive at the effective tensor for a NUM.

$$[\varepsilon_{\text{eff}}] = \begin{bmatrix} \varepsilon_{\text{o}} & 0 & 0 \\ 0 & \varepsilon_{\text{o}} & 0 \\ 0 & 0 & \varepsilon_{\text{e}} \end{bmatrix} \qquad \begin{aligned} \varepsilon_{\text{o}} &= f\varepsilon_1 + (1-f)\,\varepsilon_2 \\ \varepsilon_{\text{e}}^{-1} &= f\varepsilon_1^{-1} + (1-f)\,\varepsilon_2^{-1} \end{aligned} \tag{6}$$

Figure 2 shows two plots of the effective permittivity values as a function of fill factor. The plots contain different performance metrics for the NUM that will be derived and described in the following sections. The plot on the left displays the ordinary and extraordinary permittivity as a function of fill factor along with the strength of anisotropy defined as $\Delta\varepsilon = \varepsilon_{\text{e}} - \varepsilon_{\text{o}}$. The plot on the right shows the same ordinary and extraordinary permittivity along with the background permittivity ε and stretch parameter a that will be derived from a spatial transform in a later section of this paper.

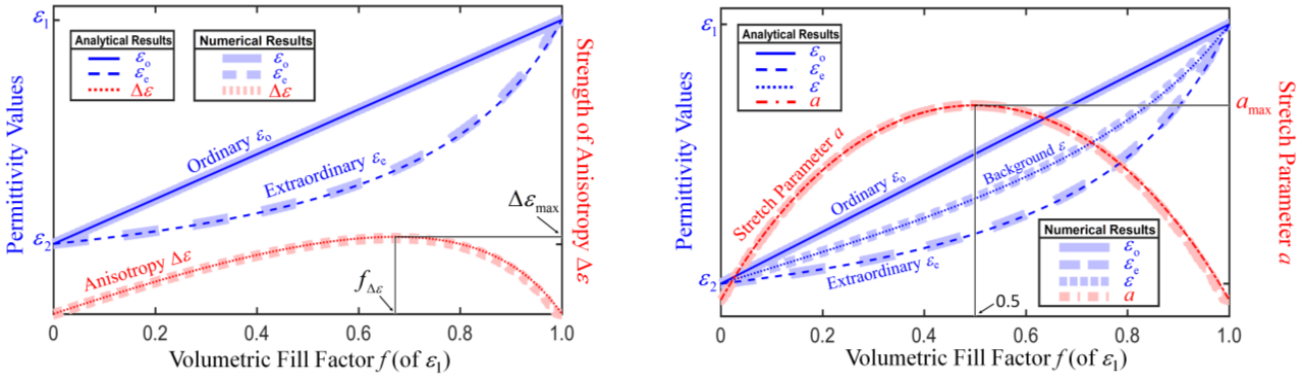

Figure 2. Plots of the effective permittivity values ε_{o} and ε_{e} vs. fill factor obtained analytically and through rigorous simulation. (a) Plot overlaid with anisotropy strength parameter $\Delta\varepsilon$. (b) Plot overlaid with the background permittivity ε and stretch parameter a.

2.2. Optimization of $\Delta\varepsilon$

Some applications, such as artificial wave plates [19, 20], are based on the difference between the extraordinary and ordinary constitutive values. The strength of the anisotropy, or birefringence, can be defined as

$$\Delta\varepsilon = \varepsilon_{\text{e}} - \varepsilon_{\text{o}}. \tag{7}$$

Positive uniaxial materials have a positive $\Delta\varepsilon$, whereas NUMs have a negative $\Delta\varepsilon$ [21, 22]. An expression to calculate $\Delta\varepsilon$ can be derived by substituting Eqs. (3) and (5) into Eq. (7). This simplifies to

$$\Delta\varepsilon = \frac{(\varepsilon_1 - \varepsilon_2)^2}{\varepsilon_1/f + \varepsilon_2/(1-f)}. \tag{8}$$

Figure 2(a) plots $\Delta\varepsilon$ as a function of fill factor. The fill factor $f_{\Delta\varepsilon}$ that maximizes $\Delta\varepsilon$ is determined from Eq. (8) using the first-derivative rule. The answer is

$$f_{\Delta\varepsilon} = \frac{1}{1 + \sqrt{\varepsilon_2/\varepsilon_1}}. \tag{9}$$

Substituting this expression for f into Eq. (8) gives an expression for the maximum possible $\Delta\varepsilon$ that occurs at the optimum fill factor $f_{\Delta\varepsilon}$. This maximum is identified in Figure 2(a) and it is clear that the maximum occurs at values of fill factor greater than 50%.

$$\Delta\varepsilon_{\max} = \varepsilon_1 + \varepsilon_2 - 2\sqrt{\varepsilon_1\varepsilon_2} \tag{10}$$

2.3. Optimization for Stretch Parameter a

Transformation optics (TO) can be used to calculate the permeability and permittivity functions that bend the fields in a manner described by a coordinate transform [14, 15]. To stretch space along the z-axis by a factor a, the following coordinate transform is used.

$$x' = x, \quad y' = y, \quad z' = z/a \tag{11}$$

Applying TO, this coordinate transform leads to the following permeability and permittivity tensor, where ε is the background permittivity

$$\left[\mu'\right] = \left[\varepsilon'\right] = \begin{bmatrix} \varepsilon a & 0 & 0 \\ 0 & \varepsilon a & 0 \\ 0 & 0 & \varepsilon/a \end{bmatrix} \tag{12}$$

Note that when $a > 1$, Eq. (12) corresponds to a negative uniaxial medium. Expressions can be derived for ε and a in terms of ε_{o} and ε_{e} by comparing Eq. (12) to Eq. (6).

$$\varepsilon = \sqrt{\varepsilon_{\mathrm{o}}\varepsilon_{\mathrm{e}}} \tag{13}$$

$$a = \sqrt{\varepsilon_{\mathrm{o}}/\varepsilon_{\mathrm{e}}} \tag{14}$$

Substituting Eqs. (3) and (5) into these expressions and simplifying puts ε and a in terms of f, ε_1, and ε_2.

$$\varepsilon = \sqrt{\frac{f\varepsilon_1 + (1-f)\,\varepsilon_2}{f\varepsilon_1^{-1} + (1-f)\,\varepsilon_2^{-1}}} \tag{15}$$

$$a = \sqrt{1 + f\,(1-f)\,\frac{(\varepsilon_1 - \varepsilon_2)^2}{\varepsilon_1\varepsilon_2}} \tag{16}$$

Figure 2(b) plots both ε and a as a function of fill factor. The first-derivative rule is used to determine the fill factor f_a that maximizes the stretching parameter a. The result is always

$$f_a = 0.5 \tag{17}$$

This is a very fortunate and convenient answer for two reasons. First, NUMs can be designed without having to know what materials they will be composed of. Second, the feature sizes of the NUM dielectric layers will always be the largest possible, which facilitates easier manufacturing. At this optimum fill factor, the background permittivity ε and stretch factor a are

$$\varepsilon\,(f_a) = \sqrt{\varepsilon_1\varepsilon_2} \tag{18}$$

$$a_{\max} = \frac{\varepsilon_1 + \varepsilon_2}{2\sqrt{\varepsilon_1\varepsilon_2}} \tag{19}$$

It is important to note that achieving this stretch factor requires both the permeability and permittivity to be the same. It is usually desired to manufacture NUMs from purely dielectric materials that do not possess a significant magnetic response. This, however, reduces the effective stretch parameter to $\sqrt{a}$. This can be understood when the effective stretch parameter a_{eff} is taken from the refractive index tensor instead of the permittivity or permeability tensor. When permeability is removed, the relation between the refractive index tensor $[n]$ and the permittivity tensor $[\varepsilon_{\mathrm{eff}}]$ is

$$[\mu] = \begin{bmatrix} 1 & 0 & 0 \\ 0 & 1 & 0 \\ 0 & 0 & 1 \end{bmatrix} \quad [n] = [\sqrt{\varepsilon_{\mathrm{eff}}}] = \begin{bmatrix} \sqrt{\varepsilon a} & 0 & 0 \\ 0 & \sqrt{\varepsilon a} & 0 \\ 0 & 0 & \sqrt{\varepsilon/a} \end{bmatrix} = \begin{bmatrix} n a_{\mathrm{eff}} & 0 & 0 \\ 0 & n a_{\mathrm{eff}} & 0 \\ 0 & 0 & n/a_{\mathrm{eff}} \end{bmatrix}. \tag{20}$$

It follows from Eq. (20) that the background refractive index n and the effective stretch parameter a_{eff} for the dielectric-only case are

$$n = \sqrt{\varepsilon}, \tag{21}$$

$$a_{\mathrm{eff}} = \sqrt{a}. \tag{22}$$

3. DESIGN & SIMULATION

3.1. Plane Wave Expansion Method Analysis

The plane wave expansion method (PWEM) was used as a rigorous method to retrieve the effective tensor parameters ε_o and ε_e [16] for a purely dielectric NUM (i.e., $\mu_r = 1$). To calculate these parameters Maxwell's equations were solved as an eigen-value problem where the eigen-value was the free space wave number squared, k_0^2. The geometry and construction of our simulation is illustrated in Figure 3. The NUM was reduced to a one-dimensional structure with periodic boundary conditions at either end of the axis. In this framework, the remaining two axes are infinitely extruded, representing the infinite planes of the NUM. The Bloch wave was set to propagate in a direction parallel to the planes as defined by the Bloch wave vector $\vec{\beta}$. To ensure the NUM is sufficiently subwavelength, the Bloch wave vector was made to have a very small magnitude (i.e., $|\vec{\beta}| \ll 0.5/a$). When solved as eigen-value problem, the effective permittivity is calculated from the Bloch wave vector and eigen-value as $\varepsilon_{\text{eff}} = (|\vec{\beta}|/k_0)^2$. Last, polarization of the Bloch wave must be considered to determine if the retrieved value of permittivity is the ordinary or extraordinary permittivity of the NUM. For the configuration shown in Figure 3, the TM mode has the electric field polarized parallel to the planes so it is the ordinary permittivity ε_o that is retrieved from the TM polarized Bloch wave. Likewise, the TE mode has the electric field polarized perpendicular to the planes so it is the extraordinary permittivity ε_e that is retrieved.

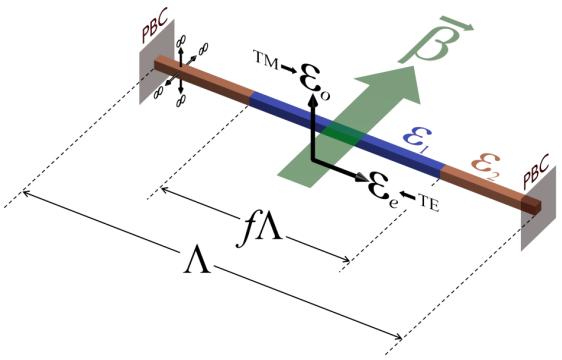

Figure 3. PWEM simulation (1D) setup showing the direction of the Bloch wave along with the electric field polarization for both TE and TM.

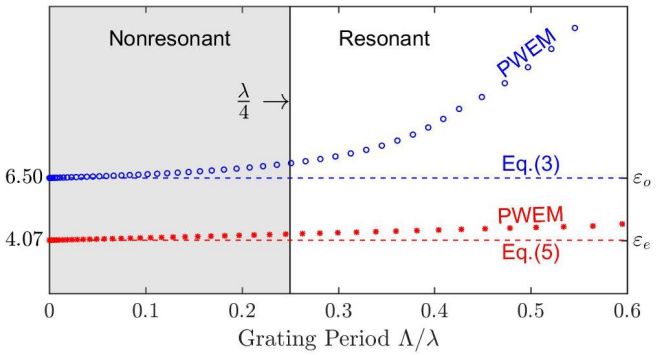

Figure 4. Simulated effective medium properties as a function of grating period Λ where $\varepsilon_{r1} = 10.5$ and $\varepsilon_{r2} = 2.5$ with a 50% fill factor. Simulations converge to the analytical equations below $\Lambda = \lambda/4$, where resonance is cutoff.

The effective parameters retrieved using the PWEM are plotted versus fill factor in Figure 2. This data is a virtual overlay onto the lines plotted using the analytical expressions derived in Section 2. This confirms the validity of the analytical expressions as long as the NUM is sufficiently subwavelength and thus nonresonant. To identify the condition for being sufficiently subwavelength, the data in Figure 4 was generated by simulating the effective tensor elements as a function of grating period Λ normalized by the wavelength λ inside the NUM. It can be observed from this plot that the effective tensor elements ε_o and ε_e converge to the values predicted by Eqs. (3) and (5), respectively, when the lattice spacing is below a quarter-wavelength $\lambda/4$ and thus this is the desired operating region. Given that the wavelength inside the NUM is $\lambda = \lambda_0/\sqrt{\varepsilon_{\text{eff}}}$, the cutoff condition can be defined as

$$\Lambda \leq \frac{\lambda_0}{4\sqrt{\varepsilon_{\text{eff}}}}. \tag{23}$$

3.2. Simulation of the Experimental Setup

To confirm the analytical equations and simulations, three NUM samples were manufactured by 3D printing and the effective parameters measured in the lab using the Nicolson-Ross-Weir (NRW)

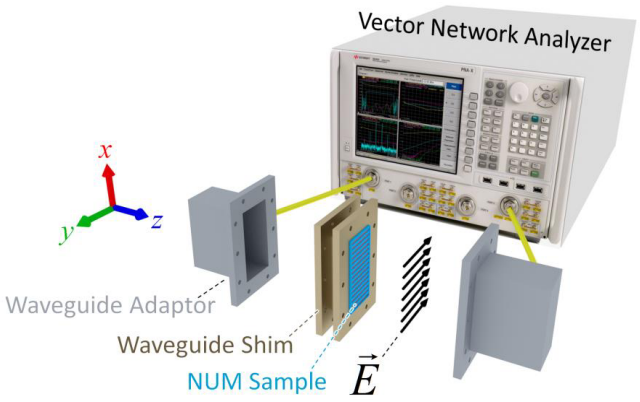

Figure 5. Experimental setup to measure the effective tensor elements of the NUMs.

technique [23, 24]. The three NUM samples were designed with an optimized for stretching parameter a because this would lead to more convenient manufacturing with a fill factor of $f = 50\%$. Figure 5 illustrates our laboratory setup for the NRW measurement technique. The NUM was inserted into a waveguide shim and placed in between two waveguide-to-coax adaptors that connected the setup to a vector network analyzer (VNA). The inside dimensions of the waveguide are $W = 109.22\,\text{mm}$ and $L = 54.61\,\text{mm}$.

To confirm this measurement technique, the experimental setup was simulated using Ansys Electronics Desktop [25]. The complex scattering parameters S_{11} and S_{21} were extracted from the simulation and imported into MATLAB where the NRW technique [26, 27] was implemented. In the waveguide configuration shown in Figure 5, the electric field is always linearly polarized parallel to the y-axis. Therefore, it is this axis that is interrogated by the setup. In order to measure all three tensor elements, three NUMs were needed with the planes oriented different directions. CAD models of these are provided in Figure 6(a). The NUMs were to be composed of high-permittivity dielectric powder and an acrylonitrile butadiene styrene (ABS) plastic. The permittivity of the materials was measured using the NRW technique to have a dielectric constant of $\varepsilon_1 = 10.5$ and $\varepsilon_2 = 2.5$, respectively. To avoid branching problems in the NRW technique, the samples were made to be as close to a quarter-wavelength thick in the z-direction as possible, but it is not necessary to be exact. Simulations were also performed to assess the cross-sensitivity to the effective tensor elements in the x and z directions, which was found to be negligible. This was accomplished by adjusting the values of the tensor elements orthogonal to the polarization of the electric field and observing any changes.

Figure 6(b) shows the retrieved parameters for two different sample simulations in Ansys Electronics Desktop as well as compares the results to what Eqs. (3) and (5) predict. The first sample was a solid homogeneous anisotropic block where the effective tensor parameters calculated with PWEM in Section 3.1, $\varepsilon_\text{o} = 6.5$ and $\varepsilon_\text{e} = 4.07$ were entered directly into the simulation as an effective medium. The second sample was a NUM composed of alternating layers of dielectric, ε_1 and ε_2, that fit perfectly into the waveguide without using an outer plastic shell, refered to as ideal NUM. The data in these plots are in very good agreement, confirming the NUM is truly behaving as an effective medium. Careful consideration was taken to ensure measurements matched simulations as closely as possible. First, the relative permittivity of both materials used for fabrication were measured experimentally. Second, care was taken to ensure the simulations replicated the experimental setup by including the outer shell that will be discussed in the manufacturing section. Third, these devices are nonresonant and so the physics is quite simple compared to traditional resonant metamaterials. The NUMs layered in the x and z directions gave the value for ordinary permittivity ε_o because the electric field was polarized parallel to the planes. The effective permittivity retrieved from the simulation was $\varepsilon_\text{o} = 6.50$. The NUM layered in the y direction gave the value for the extraordinary permittivity ε_e because the electric field was polarized perpendicular to the planes. The effective permittivity retrieved from the simulation was $\varepsilon_\text{e} = 4.04$.

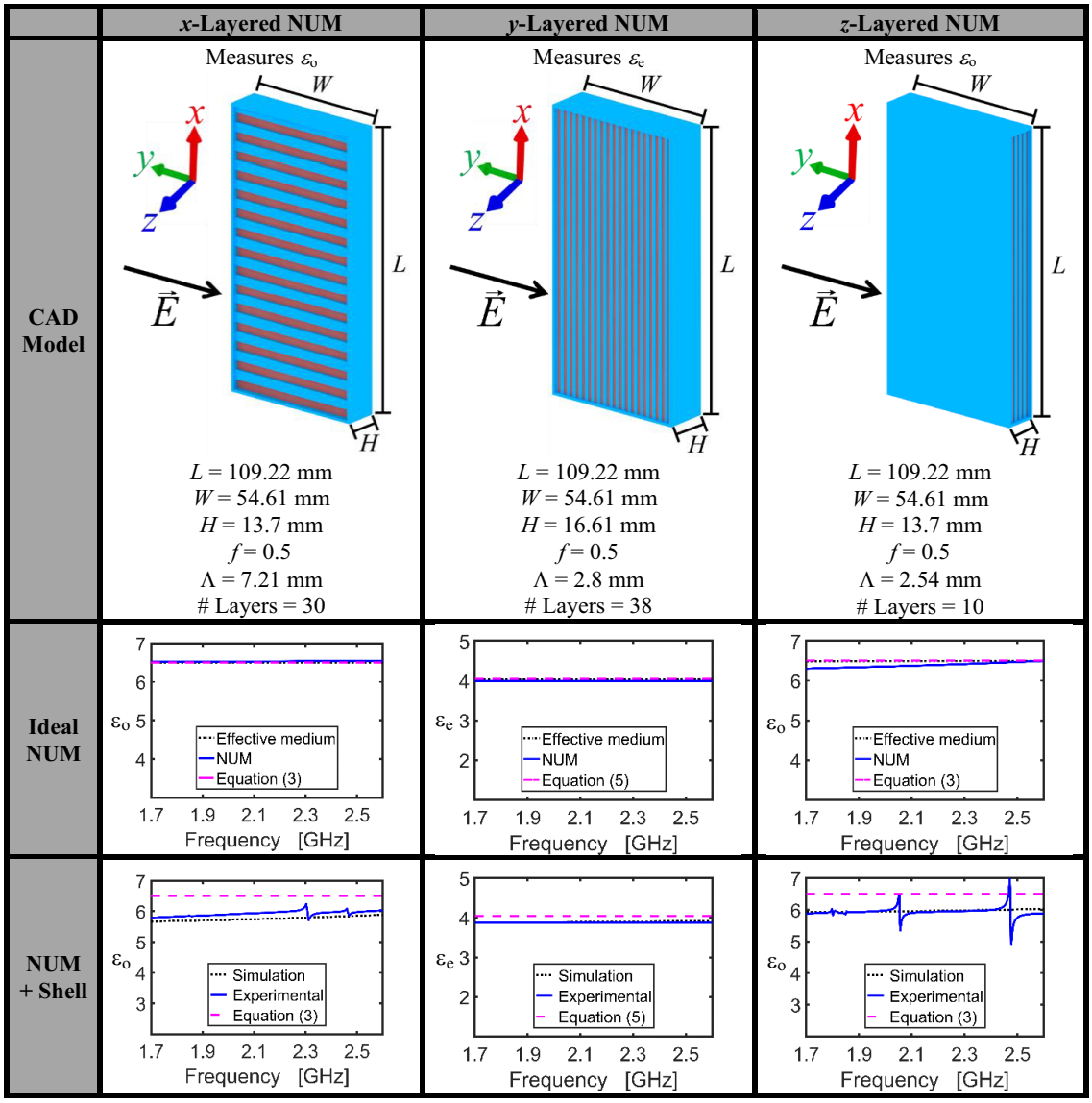

Figure 6. The NUM samples along with simulation and experimental data. (a) NUMs layered in three different directions. (b) Simulation results for NUMs without outer shell. (c) Comparison of analytical calculations, simulations, and measurements of NUMs with outer shell.

To contain the powder inside the NUM, it was necessary to include a 1 mm thick shell around the entire outside of the device. Unfortunately, the shell introduced a small defect into the samples that made it act like a weak resonant grating [28, 29] at certain frequencies. The resonances produced glitches in the retrieved parameters that appeared in both the simulations and the experiments. Figure 6(c) overlays Eqs. (3) and (5), Ansys Electronics Desktop simulation, and the experimental results for the manufactured NUMs. In this row, both the simulated and experimental NUMs included the outer shell to contain the high-permittivity powder. Adding the shell lowered the permittivity value of the experimental results compared to the analytical equations and the ideal NUM simulations. This effect of the shell was confirmed through simulation and the plots in Figure 6(c) show good agreement between these simulations and the experiments.

4. EXPERIMENTAL MEASUREMENTS

4.1. Manufacturing

As discussed previously, three NUMs with optimized stretch parameter were manufactured with the alternating planes oriented in different directions. CAD models of these devices are shown in Figure 6(a). Each NUM was manufactured using fused deposition modeling (FDM) on a Makerbot Replicator 2X. FDM was developed by Stratasys [30, 31] and is a standard method of manufacturing plastic parts by extruding filament. FDM has matured and been hybridized with other 3D printing techniques to combine plastics with metals or other dielectrics. The light blue material in the CAD models represents ABS plastic, while the red layers represent the high-permittivity dielectric powder provided by Laird Technologies [32]. To contain the powder, it was necessary to include a 1 mm thick solid plastic shell around the entire outside of the NUM. When high-permittivity materials are available for 3D printing, the entire NUM could be solid and monolithic and not require this shell. The dimensions of the three NUM designs are summarized in Figure 6(a).

After 3D printing, the NUMs were filled with the high-permittivity dielectric powder and then sealed using Plastruct plastic welder. The powder was packed as tight and uniform as possible. Photographs of one of the fabricated NUMs are shown in Figure 7. These photographs include the unfilled NUM (a), filled NUM (b), and sealed NUM (c). Once sealed, all the NUMs looked the same from the outside.

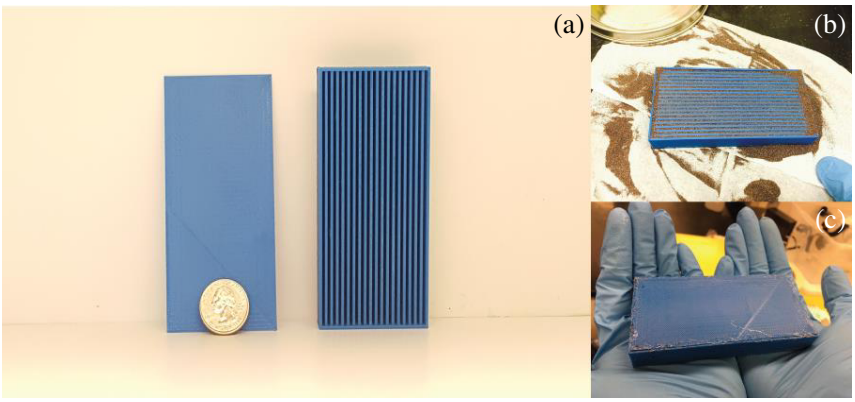

Figure 7. Photograph of fabricated NUM layered along the y direction. (a) Empty NUM. (b) NUM filled with high-permittivity dielectric powder. (c) Sealed NUM.

4.2. Measurements

One at a time, each sample was inserted into the waveguide shim and placed in between two waveguide-to-coax adaptors that connected the setup to an Agilent N5245A PNA-X vector network analyzer. WR-430 waveguides were used that operate in the frequency range of 1.7 GHz to 2.6 GHz. A photograph of the experimental setup is shown in Figure 8. The Agilent material measurement package 80971 was used. This package measured the complex scattering parameters, S_{11} and S_{21}, and applied the NRW technique extracting the permittivity and permeability. The extracted parameters were saved to a file and imported to MATLAB to compare with the simulated and analytical data. The materials possessed no magnetic response so the relative permeability was 1.0. Measurements obtained from the x- and z-layered NUMs were interpreted as the ordinary permittivity ε_{o}. Measurements taken from the y-layered NUM was interpreted as the extraordinary permittivity ε_{e}.

Figure 6(c) shows the effective tensor elements measured using this setup. The data is overlaid with the same data obtained through simulation and from analytical expressions. All data is in excellent agreement. The shell used to fabricate the NUMs was found to lower the values expected from an ideal NUM, but was a necessary component for manufacturing and measurement. There is very good agreement between the simulation of the shelled NUMs and the fabricated shelled NUMs.

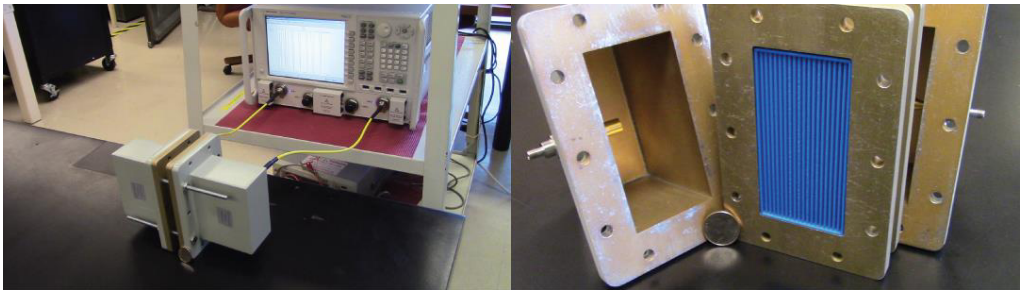

(a) (b)

Figure 8. Photographs of waveguide measurement setup. (a) Agilent N5245A PNA-X vector network analyzer connected to the waveguides. (b) Waveguide shim containing the y-layered NUM.

5. CONCLUSION

This paper outlined the physics and optimization of negative uniaxial metamaterials. The NUMs were optimized for strength of anisotropy as well as for space stretching. Analytical expressions were derived and validated by rigorous simulation and experimental measurements performed in the laboratory. To maximize the strength of the anisotropy, it is necessary to have them composed of 60% to 80% of the high-permittivity material by volume. To maximize the space stretching, it was found that duty cycle of the alternating layers is always exactly 50% regardless of the properties of the constituent materials. This is a very convenient conclusion for two reasons. First, designs can be produced without having to know the material properties. Second, manufacturing is easier because the layer thicknesses are always maximized. Last, three NUM samples were manufactured by 3D printing and measured in the lab to retrieve the effective tensor of the NUM. The three manufactured NUMs where optimized for space stretching because of the fill factor being a convenient 50%. Experiments, simulations, and analytical results were in excellent agreement confirming the physics of NUMs is well understood and that NUMs can be designed using only the analytical equations. These equations assume that the lattice spacing of the NUM is sufficiently subwavelength, where the cutoff is around $\lambda/4$. NUMs are anticipated to find applications in field-sculpting, artificial wave plates, and other 3D printed electromagnetic applications.

REFERENCES

1. Gibson, I., D. W. Rosen, and B. Stucker, *Additive Manufacturing Technologies: Rapid Prototyping to Direct Digital Manufacturing*, Springer, 2010.
2. Church, K., E. MacDonald, P. Clark, R. Taylor, D. Paul, K. Stone, M. Wilhelm, F. Medina, J. Lyke, and R. Wicker, "Printed electronic processes for flexible hybrid circuits and antennas," *2009 Flexible Electronics & Displays Conference and Exhibition*, 1–7, 2009.
3. Espalin, D., D. W. Muse, E. MacDonald, and R. B. Wicker, "3D Printing multifunctionality: Structures with electronics," *The International Journal of Advanced Manufacturing Technology*, Vol. 72, No. 5, 963–978, 2014.
4. Ketterl, T. P., Y. Vega, N. C. Arnal, J. W. I. Stratton, E. A. Rojas-Nastrucci, M. F. Córdoba-Erazo, M. M. Abdin, C. W. Perkowski, P. I. Deffenbaugh, K. H. Church, and T. M. Weller, "A 2.45 GHz phased array antenna unit cell fabricated using 3-D multi-layer direct digital manufacturing," *IEEE Transactions on Microwave Theory and Techniques*, Vol. 63, No. 12, 4382–4394, 2015.
5. Yi, J., S. N. Burokur, G. Piau, and A. Lustrac, "3D printed broadband transformation optics based all-dielectric microwave lenses," *Journal of Optics*, Vol. 18, No. 4, 044010, 2016.
6. Rumpf, R. C., J. Pazos, C. R. Garcia, L. Ochoa, and R. Wicker, "3D printed lattices with spatially variant self-collimation," *Progress In Electromagnetics Research*, Vol. 139, 1–14, 2013.

7. Hao, J., Y. Yuan, L. Ran, T. Jiang, J. A. Kong, C. T. Chan, and L. Zhou, "Manipulating electromagnetic wave polarizations by anisotropic metamaterials," *Phys. Rev. Lett.*, Vol. 99, No. 6, 063908, 2007.
8. Pendry, J. B., D. Schurig, and D. R. Smith, "Controlling electromagnetic fields," *Science*, Vol. 312, No. 5781, 1780–1782, 2006.
9. Rumpf, R. C., C. R. Garcia, H. H. Tsang, J. E. Padilla, and M. D. Irwin, "Electromagnetic isolation of a microstrip by embedding in a spatially variant anisotropic metamaterial," *Progress In Electromagnetics Research*, Vol. 142, 243–260, 2013.
10. Garcia, C. R., J. Correa, D. Espalin, J. H. Barton, R. C. Rumpf, R. Wicker, and V. Gonzalez, "3D printing of anisotropic metamaterials," *Progress In Electromagnetics Research Letters*, Vol. 34, 75–82, 2012.
11. Datta, S., C. T. Chan, K. M. Ho, and C. M. Soukoulis, "Effective dielectric constant of periodic composite structures," *Physical Review B*, Vol. 48, 14936, 1993.
12. Lalanne, P. and J. Hugonin, "High-order effective-medium theory of subwavelength gratings in classical mounting: Application to volume holograms," *J. Opt. Soc. Am. A*, Vol. 15, No. 7, 1843–1851, 1998.
13. Grann, E. B., M. G. Moharam, and D. A. Pommet, "Artificial uniaxial and biaxial dielectrics with use of two-dimensional subwavelength binary gratings," *J. Opt. Soc. Am. A*, Vol. 11, 2695–2703, 1994.
14. Berry, E. A., J. J. Gutierrez, and R. C. Rumpf, "Design and simulation of arbitrarily-shaped transformation optic devices using a simple finite-difference method," *Progress In Electromagnetics Research B*, Vol. 68, 1–16, 2016.
15. Kwon, D. H. and D. H. Werner, "Transformation electromagnetics: An overview of the theory and applications," *IEEE Antennas and Propagation Magazine*, Vol. 52, No. 1, 24–46, 2010.
16. Leung, K. and Y. Liu, "Photon band structures: The plane-wave method," *Physical Review B*, Vol. 41, 10188, 1990.
17. Flanders, D. C., "Submicrometer periodicity gratings as artificial anisotropic dielectrics," *Appl. Phys. Lett.*, Vol. 42, No. 6, 492–494, 1983.
18. Lalanne, P. and D. Lemercier-Lalanne, "Depth dependence of the effective properties of subwavelength gratings," *J. Opt. Soc. Am. A*, Vol. 14, No. 2, 450–459, 1997.
19. Kikuta, H., Y. Ohira, and K. Iwata, "Achromatic quarter-wave plates using the dispersion of form birefringence," *Appl. Opt.*, Vol. 36, 1566–1572, 1997.
20. Van Vliet, A. H. F. and T. de Graauw, "Quarter wave plates for submillimeter wavelengths," *Int. J. Infrared Millim. Waves*, Vol. 2, No. 3, 465–477, 1981.
21. Born, M. and E. Wolf, "Light propagation in uniaxial crystals," *Principles in Optics*, 680, 1970.
22. Rumpf, R. C., "Chapter three — Engineering the dispersion and anisotropy of periodic electromagnetic structures," *Solid State Physics*, Vol. 66, 213–300, 2015.
23. Nicolson, A. M. and G. F. Ross, "Measurement of the intrinsic properties of materials by time-domain techniques," *IEEE Transactions on Instrumentation and Measurement*, Vol. 19, No. 4, 377–382, 1970.
24. Weir, W. B., "Automatic measurement of complex dielectric constant and permeability at microwave frequencies," *Proceedings of the IEEE*, Vol. 62, No. 1, 33–36, 1974.
25. Ansys, http://www.ansys.com/Products/Electronics/, Ansys Electromagnetics.
26. Rumpf, R. C., http://emlab.utep.edu/ee5390em21/Lecture%2015%20–%20Homogenization%20-and%20parameter%20retrieval.pdf, Homogenization and Parameter Retrieval.
27. Vicente, A. N., G. M. Dip, and C. Junqueira, "The step by step development of NRW method," *2011 SBMO/IEEE MTT-S International Microwave and Optoelectronics Conference (IMOC 2011)*, 738–742, 2011.
28. Wang, S. S., G. Moharam, R. Magnusson, and J. S. Bagby, "Guided-mode resonances in planar dielectric-layer diffraction gratings," *J. Opt. Soc. Am. A*, Vol. 7, 1470–1474, 1990.

29. Wang, S. S. and R. Magnusson, "Theory and applications of guided-mode resonance filters," *Appl. Opt.*, Vol. 32, 2606–2613, 1993.
30. Stratasys, http://www.stratasys.com/3d-printers/technologies/fdm-technology, Fused deposition modeling technology.
31. Steven, A., "Rapid prototyping is coming of age," *Mechanical Engineering*, Vol. 117, No. 7, 62, 1995.
32. Laird Technologies, http://www.lairdtech.com, Laird HiK Powder.